Research Article | Vol. 26, No. 4 | 19 Feb 2018 | OPTICS EXPRESS 4751
Optics EXPRESS

Nonlinear dynamics of solitary and optically injected two-element laser arrays with four different waveguide structures: a numerical study

NIANQIANG LI,[1] H. SUSANTO,[2] B. R. CEMLYN,[1] I. D. HENNING,[1,*] AND M. J. ADAMS[1]

[1]*School of Computer Science and Electronic Engineering, University of Essex, Wivenhoe Park, Colchester CO4 3SQ, UK*
[2]*Department of Mathematical Sciences, University of Essex, Wivenhoe Park, Colchester CO4 3SQ, UK*
**idhenn@essex.ac.uk*

Abstract: We study the nonlinear dynamics of solitary and optically injected two-element laser arrays with a range of waveguide structures. The analysis is performed with a detailed direct numerical simulation, where high-resolution dynamic maps are generated to identify regions of dynamic instability in the parameter space of interest. Our combined one- and two-parameter bifurcation analysis uncovers globally diverse dynamical regimes (steady-state, oscillation, and chaos) in the solitary laser arrays, which are greatly influenced by static design waveguiding structures, the amplitude-phase coupling factor of the electric field, i.e. the linewidth-enhancement factor, as well as the control parameter, e.g. the pump rate. When external optical injection is introduced to one element of the arrays, we show that the whole system can be either injection-locked simultaneously or display rich, different dynamics outside the locking region. The effect of optical injection is to significantly modify the nature and the regions of nonlinear dynamics from those found in the solitary case. We also show similarities and differences (asymmetry) between the oscillation amplitude of the two elements of the array in specific well-defined regions, which hold for all the waveguiding structures considered. Our findings pave the way to a better understanding of dynamic instability in large arrays of lasers.

OCIS codes: (140.5960) Semiconductor lasers; (190.3100) Instabilities and chaos; (140.3520) Lasers, injection-locked; (140.2010) Diode laser arrays; (230.7400) Waveguides, slab.

References and links

1. N. Blackbeard, S. Wieczorek, H. Erzgräber, and P. S. Dutta, "From synchronization to persistent optical turbulence in laser arrays," Physica D **286–287**, 43–58 (2014).
2. W.-P. Huang, "Coupled-mode theory for optical waveguides: an overview," J. Opt. Soc. Am. A **11**(3), 963–983 (1994).
3. D. F. Siriani, K. D. Choquette, and P. S. Carney, "Stochastic coupled mode theory for partially coherent laser arrays," J. Opt. Soc. Am. A **27**(3), 501–508 (2010).
4. J. Xu and Y. Chen, "General coupled mode theory in non-Hermitian waveguides," Opt. Express **23**(17), 22619–22627 (2015).
5. E. Kapon, J. Katz, and A. Yariv, "Supermode analysis of phase-locked arrays of semiconductor lasers," Opt. Lett. **9**(4), 125–127 (1984).
6. E. Marom, O. G. Ramer, and S. Ruschin, "Relation between normal-mode and coupled-mode analyses of parallel waveguides," IEEE J. Quantum Electron. **20**(12), 1311–1319 (1984).
7. W. W. Chow, "Effects of spatial gain variation in an index-guided semiconductor laser array," J. Opt. Soc. Am. B **4**(3), 324–328 (1987).
8. O. Hess and E. Scholl, "Spatio-temporal dynamics in twin-stripe semiconductor lasers," Physica D **70**(1–2), 165–177 (1994).
9. N. Blackbeard, H. Erzgräber, and S. Wieczorek, "Shear-induced bifurcations and chaos in models of three coupled lasers," SIAM J. Appl. Dyn. Syst. **10**(2), 469–509 (2011).

#315176 https://doi.org/10.1364/OE.26.004751
Journal © 2018 Received 7 Dec 2017; revised 23 Jan 2018; accepted 24 Jan 2018; published 14 Feb 2018

Optics EXPRESS

10. H. Erzgräber, S. Wieczorek, and B. Krauskopf, "Dynamics of two laterally coupled semiconductor lasers: strong- and weak-coupling theory," Phys. Rev. E Stat. Nonlin. Soft Matter Phys. **78**(6), 066201 (2008).
11. S. S. Wang and H. G. Winful, "Dynamics of phase-locked semiconductor laser arrays," Appl. Phys. Lett. **52**(21), 1774–1776 (1988).
12. H. G. Winful and S. S. Wang, "Stability of phase-locking in coupled semiconductor laser arrays," Appl. Phys. Lett. **53**(20), 1894–1896 (1988).
13. H. G. Winful and L. Rahman, "Synchronized chaos and spatiotemporal chaos in arrays of coupled lasers," Phys. Rev. Lett. **65**(13), 1575–1578 (1990).
14. H. Erzgräber, S. Wieczorek, and B. Krauskopf, "Locking behavior of three coupled laser oscillators," Phys. Rev. E Stat. Nonlin. Soft Matter Phys. **80**(2), 026212 (2009).
15. H. Lamela, M. Leones, G. Carpintero, C. Simmendinger, and O. Hess, "Analysis of the dynamics behavior and short-pulse modulation scheme for laterally coupled diode lasers," IEEE J. Sel. Top. Quantum Electron. **7**(2), 192–200 (2001).
16. P. Ru, P. K. Jakobsen, J. V. Moloney, and R. A. India, "Generalized coupled-mode model for the multistripe index-guided laser arrays," J. Opt. Soc. Am. B **10**(3), 507–515 (1993).
17. R. Santos and H. Lamela, "Experimental observation of chaotic dynamics in two coupled diode lasers through lateral model locking," IEEE J. Quantum Electron. **45**(11), 1490–1494 (2009).
18. G. A. Wilson, R. K. DeFreez, and H. G. Winful, "Modulation of phased-array semiconductor lasers at K-band frequencies," IEEE J. Quantum Electron. **27**(6), 1696–1704 (1991).
19. S. T. M. Fryslie, Z. Gao, H. Dave, B. J. Thompson, K. Lakomy, S. Lin, P. Decker, D. McElfresh, J. E. Schutt-Aine, and K. D. Choquette, "Modulation of coherently-coupled phased photonic crystal vertical cavity laser arrays," IEEE J. Sel. Top. Quantum Electron. **23**(6), 1700409 (2017).
20. Z. Gao, S. T. M. Fryslie, B. J. Thompson, P. Scott Carney, and K. D. Choquette, "Parity-time symmetry in coherently coupled vertical cavity laser arrays," Optica **4**(3), 323–329 (2017).
21. J. Shena, J. Hizanidis, V. Kovanis, and G. P. Tsironis, "Turbulent chimeras in large semiconductor laser arrays," Sci. Rep. **7**, 42116 (2017).
22. Y. Kominis, V. Kovanis, and T. Bountis, "Controllable asymmetric phase-locked states of the fundamental active photonic dimer," Phys. Rev. A **96**(4), 043836 (2017).
23. K. E. Chlouverakis and M. J. Adams, "Stability maps of injection-locked laser diodes using the largest Lyapunov exponent," Opt. Commun. **216**(4-6), 405–412 (2003).
24. J. P. Toomey, D. M. Kane, S. Valling, and A. M. Lindberg, "Automated correlation dimension analysis of optically injected solid state lasers," Opt. Express **17**(9), 7592–7608 (2009).
25. J. P. Toomey, A. Argyris, C. McMahon, D. Syvridis, and D. M. Kane, "Time-scale independent permutation entropy of a photonic integrated Device," J. Lightwave Technol. **35**(1), 88–95 (2017).
26. S. Valling, T. Fordell, and A. M. Lindberg, "Maps of the dynamics of an optically injected solid-state laser," Phys. Rev. A **72**(3), 033810 (2005).
27. T. B. Simpson, J. M. Liu, K. F. Huang, and K. Tai, "Nonlinear dynamics induced by external optical injection in semiconductor lasers," Quantum Semiclassic. Opt. **9**(5), 765–784 (1997).
28. S. Wieczorek, B. Krauskopf, T. B. Simpson, and D. Lenstra, "The dynamical complexity of optically injected lasers," Phys. Rep. **416**(1-2), 1–128 (2005).
29. E. J. Doedel, A. R. Champneys, T. Fairgrieve, Y. Kuznetsov, B. Oldeman, R. Pfaffenroth, B. Sandastede, X. Wang, and C. Zhang, *AUTO-07p: Continuation and Bifurcation Software for Ordinary Differential Equations* (Concordia University, Montreal, 2008).
30. N. Q. Li, H. Susanto, B. R. Cemlyn, I. D. Henning, and M. J. Adams, "Stability and bifurcation analysis of spin-polarized vertical-cavity surface-emitting lasers," Phys. Rev. A **96**(1), 013840 (2017).
31. F. Rogister and M. Blondel, "Dynamics of two mutually delay-coupled semiconductor lasers," Opt. Commun. **239**(1), 173–180 (2004).
32. A. Argyris, D. Syvridis, L. Larger, V. Annovazzi-Lodi, P. Colet, I. Fischer, J. García-Ojalvo, C. R. Mirasso, L. Pesquera, and K. A. Shore, "Chaos-based communications at high bit rates using commercial fibre-optic links," Nature **438**(7066), 343–346 (2005).
33. A. Uchida, K. Amano, M. Inoue, K. Hirano, S. Naito, H. Someya, I. Oowada, T. Kurashige, M. Shiki, S. Yoshimori, K. Yoshimura, and P. Davis, "Fast physical random bit generation with chaotic semiconductor lasers," Nat. Photonics **2**(12), 728–732 (2008).
34. M. Sciamanna and K. A. Shore, "Physics and applications of laser diode chaos," Nat. Photonics **9**(3), 151–162 (2015).
35. D. Rontani, D. Choi, C.-Y. Chang, A. Locquet, and D. S. Citrin, "Compressive sensing with optical chaos," Sci. Rep. **6**(1), 35206 (2016).
36. P. Li, J. Zhang, L. Sang, X. Liu, Y. Guo, X. Guo, A. Wang, K. Alan Shore, and Y. Wang, "Real-time online photonic random number generation," Opt. Lett. **42**(14), 2699–2702 (2017).
37. S. C. Chan, S. K. Hwang, and J. M. Liu, "Period-one oscillation for photonic microwave transmission using an optically injected semiconductor laser," Opt. Express **15**(22), 14921–14935 (2007).
38. M. J. Adams, N. Q. Li, B. R. Cemlyn, H. Susanto, and I. D. Henning, "Effects of detuning, gain-guiding and index antiguiding on the dynamics of two laterally-coupled semiconductor lasers," Phys. Rev. A **95**(5), 053869 (2017).

Optics EXPRESS

39. N. Q. Li, H. Susanto, B. R. Cemlyn, I. D. Henning, and M. J. Adams, "Locking bandwidth of two laterally-coupled lasers subjected to optical injection," Sci. Rep. **8**(109), 1–10 (2018).
40. S. Yanchuk, K. R. Schneider, and L. Recke, "Dynamics of two mutually coupled semiconductor lasers: instantaneous coupling limit," Phys. Rev. E Stat. Nonlin. Soft Matter Phys. **69**(5), 056221 (2004).
41. L. Rahman and H. G. Winful, "Nonlinear dynamics of semiconductor laser arrays: a mean field model," IEEE J. Quantum Electron. **30**(6), 1405–1416 (1994).
42. F. Rogister and J. García-Ojalvo, "Symmetry breaking and high-frequency periodic oscillations in mutually coupled laser diodes," Opt. Lett. **28**(14), 1176–1178 (2003).
43. A. Hohl and A. Gavrielides, "Bifurcation cascade in a semiconductor laser subject to optical feedback," Phys. Rev. Lett. **82**(6), 1148–1151 (1999).
44. J. Ohtsubo, *Semiconductor Lasers: Stability, Instability, and Chaos* (Springer, 2012).
45. G. A. Gottwald and I. Melbourne, "On the implementation of the 0–1 test for chaos," SIAM J. Appl. Dyn. Syst. **8**(1), 129–145 (2009).
46. C. M. Long, L. Mutter, B. Dwir, A. Mereuta, A. Caliman, A. Sirbu, V. Iakovlev, and E. Kapon, "Optical injection locking of transverse modes in 1.3-μm wavelength coupled-VCSEL arrays," Opt. Express **22**(18), 21137–21144 (2014).

1. Introduction

Considerable progress has been made over the past few years in understanding the dynamic properties of arrays of semiconductor lasers that are coupled by the overlap of their evanescent fields (see, for example [1], and references therein). Coupled mode theory [2] has served as a standard analysis tool for many decades, with further refinements being made to account for specific situations, e.g. partially coherent arrays [3] and non-Hermitian waveguides [4]. The method variously termed as supermode [5], normal-mode [6], or composite cavity [7] model is also well-established. More complex numerical models that include spatial and temporal effects can also be applied to specific laser arrays where the parameters are well-defined [8]. Nevertheless in the weak coupling regime, coupled mode theory, as the simplest modeling approach, has been demonstrated to be sufficiently accurate [9,10] and therefore this modeling method will be utilized in this work.

Studies of laterally-coupled semiconductor lasers based on a range of structures have found that these devices are intrinsically unstable under certain conditions and can even develop complicated chaotic oscillations [8–17]. These studies have motivated research on novel physical phenomena, e.g. resonance frequency enhancement [18,19], gain tuning and parity-time symmetry breaking [20], turbulent chimeras [21], and phase-locked state asymmetry related to gain and loss in the two lasers [22]. While studies have addressed in some detail separately the steady-state operation or dynamic instability in these devices, much less work has been devoted to drawing a more complete picture of the dynamics evolution of the system in the parameter space.

A global view of the temporal dynamics of laser systems can be presented in terms of two-dimensional maps delineating different dynamical regions. Methods for identifying these regions include the use of largest Lyapunov exponent (or spectrum) [23], correlation dimension [24], permutation entropy [25], the maxima of intensity time series [26], and optical (radio frequency) spectra [27]. Additionally the use of bifurcation analysis [28] which can be based on either a numerical path continuation method or a direct numerical simulation has proved very effective. Bifurcation diagrams (BDs) of various bifurcation curves (saddle-node, Pitchfork, Hopf, Torus, period-doubling, saddle-node of limit cycle and so on) can be revealed with the help of standard continuation package (such as AUTO [29]) although some care is needed when interpreting results. Alternatively high-resolution BDs obtained through measuring the number of extrema of intensity time series in a direct numerical simulation have proved to be the single most effective way to illustrate different dynamical regions [30,31]. Such an approach provides an in-depth understanding of various dynamic regions and the underlying mechanism of the transition between the boundaries. This is crucial for rapidly finding the appropriate working point for diverse environments that require the generation of optical chaos [32–36], or by contrast that target stable microwave oscillations

Optics EXPRESS

[37], or even stable steady-state operation. Thus in this paper we focus on the use of bifurcation analysis of direct simulations to identify dynamical regions.

In a recent theoretical and analytical investigation of a laterally-coupled two-element laser array we have studied the existence and stability of the phase-locked solutions, confined by the principal bifurcation curves, i.e., saddle-node and Hopf, in the plane of detuning versus coupling rate for four representative laser waveguide structures, ranging from those with purely real guidance to a combination of index antiguiding and gain-guiding [38]. By doing so, we have revealed a periodicity of behavior with laser separation that was overlooked in the literature. More recently we extended this work in a study of optical injection into one element of the laser array where we focused on a detailed and comprehensive analysis of locking conditions [39]. However, the basic nature of the dynamical properties in solitary and optically injected laterally-coupled laser arrays outside the narrow locking regions have not been examined. Thus here we present a more complete theoretical investigation of dynamics in laterally-coupled pairs of lasers, with and without injection for different waveguide structures. We use one- and two-dimensional BDs to identify different dynamical regions including steady-state, periodicity, and chaos. We highlight the influence of system parameters including the waveguiding structures, linewidth-enhancement factor and the pump rate. Finally we examine the symmetry in the output of the two-laser array in the presence of optical injection into one element.

2. Theoretical model

We follow the configuration illustrated schematically in Fig. 1 of [38], and consider two identical laser waveguides, A and B, each of width $2a$, with an edge-to-edge separation of $2d$, mutually coupled through the evanescent tails of their fields. An additional degree of freedom is introduced whereby laser A is subject to continuous-wave optical injection from a master laser whose frequency can be detuned relative to those of the two-element laser array [39].

The system of dimensionless coupled-mode equations can be written as (please refer to [39] for the mathematical details of the derivation of the rate equations)

$$\frac{dY_A}{dt}=\frac{1}{2\tau_p}(M_A-1)Y_A+Y_B(\eta_r\sin\phi-\eta_i\cos\phi)+\frac{K_{inj}}{\tau_N}\cos\phi_A, \tag{1}$$

$$\frac{dY_B}{dt}=\frac{1}{2\tau_p}(M_B-1)Y_B-Y_A(\eta_r\sin\phi+\eta_i\cos\phi), \tag{2}$$

$$\frac{d\phi_A}{dt}=\frac{\alpha_H}{2\tau_p}(M_A-1)-(\omega-\Omega_A)-\frac{Y_B}{Y_A}(\eta_r\cos\phi+\eta_i\sin\phi)-\frac{K_{inj}}{\tau_N Y_A}\sin\phi_A-\Delta\omega, \tag{3}$$

$$\frac{d\phi}{dt}=\frac{\alpha_H}{2\tau_p}(M_B-M_A)+\Delta\Omega-\eta_r\cos\phi\left(\frac{Y_A}{Y_B}-\frac{Y_B}{Y_A}\right)+\eta_i\sin\phi\left(\frac{Y_A}{Y_B}+\frac{Y_B}{Y_A}\right)+\frac{K_{inj}}{\tau_N Y_A}\sin\phi_A, \tag{4}$$

$$\frac{dM_{A,B}}{dt}=\frac{1}{\tau_N}\left[Q_{A,B}-M_{A,B}\left(1+Y_{A,B}^2\right)\right], \tag{5}$$

where the subscript A, B stands for laser A, B, $Y_{A,B}$ are the normalized field amplitudes, $\phi_{A,B}$ are the corresponding phases, $M_{A,B}$ are the normalized carrier densities, ϕ $(=\phi_B-\phi_A)$ is the phase difference, and $\Delta\Omega=\Omega_B-\Omega_A$ is the built-in frequency offset between the cavity

Optics EXPRESS

resonances of the two coupled lasers in the absence of injection. The dimensionless variables $M_{A,B}$ and $Q_{A,B}$ are defined as follows

$$M_{A,B} = 1 + \frac{c}{n_g}\Gamma a_{diff}\tau_p\left(N_{A,B} - N_{A,Bth}\right), \tag{6}$$

$$Q_{A,B} = 1 + \frac{c}{n_g}\Gamma a_{diff}\tau_p\left(P_{A,B}\tau_N - N_{A,Bth}\right). \tag{7}$$

In these equations, η_r and η_i are the real and the imaginary parts of the complex coupling rate η; in Eq. (14) of [38] this rate is expressed in terms of parameters C_η, C_θ (found from numerical integration) and W_r, W_i which are the real and imaginary parts of the transverse propagation constant in the regions outside the cores of waveguides A and B. Other parameters are the speed of light c, the group index n_g, the optical confinement factor Γ, the differential gain a_{diff}, the linewidth-enhancement factor α_H, the pumping rate $P_{A,B}$, the photon lifetime τ_p, the carrier lifetime τ_N, the threshold gain g_{th}, and the threshold carrier concentration N_{th} ($= N_0 + n_g/\Gamma c a_{diff}\tau_p$ where N_0 is the transparency carrier concentration). Here we define $\Delta\omega = \omega_{inj} - \omega$, with ω_{inj} as the injected angular frequency and ω as the free-running angular frequency of the total electric field of the system in the absence of injection. K_{inj} represents the dimensionless injection level and is mathematically defined as

$$K_{inj} = \sqrt{\frac{c a_{diff}\tau_N}{n}}\, k_{inj} E_{inj}\tau_N, \tag{8}$$

where n is the refractive index and k_{inj} is the coupling rate for the injected signal E_{inj}. For a solitary pair of the laterally-coupled semiconductor lasers, i.e., in the absence of injection, $K_{inj} = k_{inj} = 0$ and $\Delta\omega = 0$.

Table 1. Values of key parameters for modelling, using material parameter values given in [38].

Δn_r	g_{th} (cm^{-1})	Δn_i	W_r	W_i	C_Q	C_η (ns^{-1})	C_θ (rad)
0.00097	87.7	0	1.26	0	11.4	83.6	0
0.0005	90.6	0.000937	1.09	0.896	11.0	90.2	0.233
0	99.3	0.00103	0.795	1.22	10.1	91.9	0.294
–0.0005	108	0.00112	0.604	1.61	9.26	96.3	0.183

In the direct numerical simulations, a fourth-order Runge-Kutta algorithm has been used to solve Eqs. (1)-(5). The following set of parameter values is considered [38,39]: $a = 4$ μm, $a_{diff} = 1\times10^{-15}$ cm^2, $N_0 = 1\times10^{18}$ cm^{-3}, $\tau_N = 1.0$ ns, $\tau_p = 1.53$ ps, and $n = 3.4$. These values are fixed throughout the current study as they are typical for laterally-coupled semiconductor lasers. We restrict attention to the case of equal pumping in each laser, so that $P \equiv P_A = P_B$. The pump rate, expressed in terms of the ratio of its threshold value P/P_{th}, and the linewidth-enhancement α_H are varied for the purpose of clarifying their effects. We consider $P = 1.1P_{th}$ and $\alpha_H = 2$, unless otherwise specified. Moreover, for consistency we study the influence of waveguiding structures based on the cases analyzed in [38,39], summarized below in Table 1. The first is purely real index guiding, the second positive index guiding with gain-guiding, the third pure gain guiding (no built-in index guiding) and the last index antiguiding with gain-

Optics EXPRESS

guiding . Although we assume the two lasers are nominally identical, we do allow for a static difference in lasing frequency ($\Delta\Omega/2\pi$) between them which might occur in practice either unintentionally as a result of small fabrication variations or by design. We refer to this as the 'offset frequency', or simply as the 'offset'.

3. Solitary case

3.1 One-parameter bifurcation diagrams

In this section, dynamics and some bifurcation scenarios of a solitary laser array consisting of two laterally-coupled semiconductor lasers are briefly introduced. It is known that two laterally-coupled lasers support steady-state solutions under appropriate conditions [12,16,38]. To start with, we consider the case of the real index guide specified in the first line of Table 1, where the two lasers have identical parameters. There exist stable steady-state solutions with identical laser output for sufficiently large laser separation (weak coupling). As the laser separation decreases, they lose stability and give rise to a stable limit cycle because of a supercritical Hopf bifurcation, and even undergo other further bifurcations leading to complex oscillatory dynamics. It is worth noting that these steady-state solutions can also disappear through a collision in a saddle-node bifurcation when a frequency offset between the two lasers is taken into account [38,40]. Figure 1 presents some examples of intensity time series of the two laterally-coupled lasers in the sequence of increasing laser separation ratio. It is clearly seen that this laser system yields rich dynamics, including Fig. 1(a) chaos, 1(b) quasiperiodicity, 1(c) periodicity and 1(d) steady state, as the control parameter (i.e. d/a in Fig. 1) is varied.

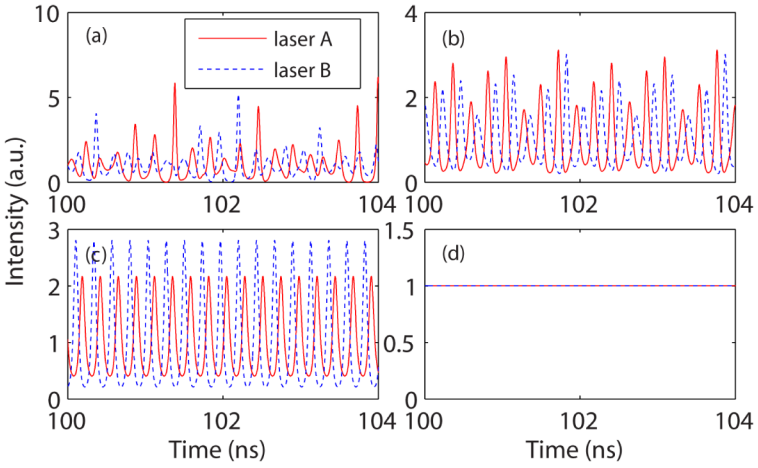

Fig. 1. Intensity time series of a solitary two-element laser array where the laser separation ratio varies from (a) $d/a = 1.0$, (b) 1.3, (c) 1.6 to (d) 2.5. Other parameters are $P = 1.1P_{th}$, offset $\Delta\Omega/2\pi = 0$ GHz , and $\alpha_H = 2$. Solid red lines represent laser A, and broken blue lines stand for laser B.

Interestingly, the symmetry breaking in periodic solutions occurs for certain large values of d/a in our system, as shown in Fig. 1(c), where both lasers output period-one oscillation at a frequency close to the relaxation resonance frequency (ROF) but with different amplitudes ($f_{ROF} = 4.5$ GHz at $P = 1.1P_{th}$ for this waveguide). This symmetry-breaking phenomenon has been observed in mutually coupled laser diodes regardless of whether the coupling is instantaneous or not [41, 42]; however, the oscillation frequency in the case of time-delayed coupling was closely related to the inverse of the time of flight between the lasers. Intuitively,

Optics EXPRESS

the appearance of symmetry breaking originates from the coexistence of several attractors (multistability), so the opposite case of Fig. 1(c) could occur depending upon the initial conditions chosen. In other words, whilst we see here that laser B has a larger amplitude than that of laser A, one can expect that laser A has a larger amplitude than that of laser B for the same parameters but another choice of initial conditions.

In Fig. 1 one can also notice that in most cases the two elements of the laser array do not necessarily oscillate precisely in phase or antiphase. Instead, they operate in an intermediate oscillatory regime characterized by a relative phase difference in the interval (0°, 180°) [see Figs. 1(b) and 1(c)], thereby consistent with results reported for two mutually coupled semiconductor lasers in the limit of instantaneous coupling [40]. In contrast, we show in Fig. 2 that by appropriately choosing the control parameters and waveguding structure, simulations produce stable antiphase and in-phase periodic solutions with the same frequency and amplitude.

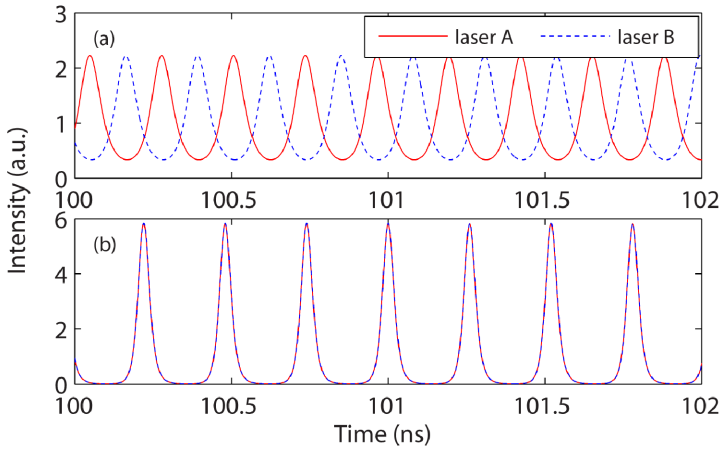

Fig. 2. Examples of antiphase and in-phase solutions in the solitary two-element laser array. (a) structure of first line in Table 1 with offset $\Delta\Omega/2\pi = 0$ GHz and $d/a = 1.85$; (b) structure of second line in Table 1 with $\Delta\Omega/2\pi = -5$ GHz and $d/a = 1.85$. Other parameters are $P = 1.1P_{th}$ and $\alpha_H = 2$.

For the results considered so far the control parameter, i.e., the laser separation ratio d/a in our case, was kept constant. We next examine the system behavior as the laser separation is varied. Figures 3(a1)-3(d1) show the BDs as a function of the laser separation ratio d/a for the four cases listed in Table 1, other parameters of $P = 1.1P_{th}$, $\alpha_H = 2$ and zero offset are kept constant. In these BDs a single dot indicates steady-state operation (locking), two or more distinct dots mean periodic oscillations, while many closely spaced dots stand for complex dynamics. Clear variations on the behavior can be seen, and typical examples of intensity time series can be seen in Figs. 1 and 2. Here in all cases shown in Figs. 3(a1)-3(d1), the system becomes unstable via a Hopf bifurcation and undergoes quasiperiodic routes to chaos. For the interval of d/a considered in this figure, one can see different windows of steady state and complex dynamics, especially in the cases of pure gain-guiding ($\Delta n = 0.0$) [Fig. 3(c1)] and real index antiguide with $\Delta n = -0.0005$ and gain-guiding [Fig. 3(d1)]. This bifurcation cascade between apparently stable and unstable regions can be predicted using the stability diagram consisting of saddle-node and Hopf bifurcations [38] and was reported also in an external-cavity semiconductor laser [43] and mutually delay-coupled semiconductor lasers [31], where the dynamics change occurs between several different adjacent cavity

Optics EXPRESS

modes. In contrast, in our case this cascade motion is attributed to the switching between in-phase and antiphase solutions and their dynamic evolution [38]. In Figs. 3(a2)-3(d2), BDs are shown for a larger value of pump ratio $P = 2P_{th}$. As can be seen, the intervals of d/a for sustained complex dynamics become much smaller and even disappears for the cases of purely real index guide with $\Delta n = 0.000971$ [Fig. 3(a2)] and real index guide with $\Delta n = 0.0005$ and gain-guiding [Fig. 3(b2)].

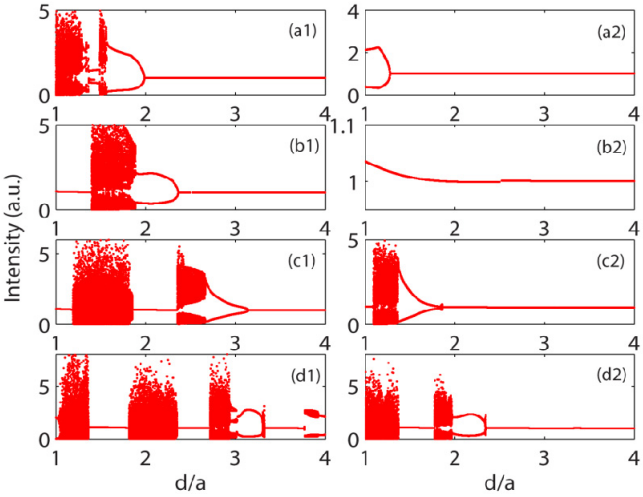

Fig. 3. One-parameter BDs as a function of laser separation d/a, calculated from laser A for offset $\Delta\Omega/2\pi = 0$ GHz and $\alpha_H = 2$ in the solitary two-element laser array. Those for laser B are similar. (a1-d1) $P = 1.1P_{th}$; (a2-d2) $P = 2P_{th}$.

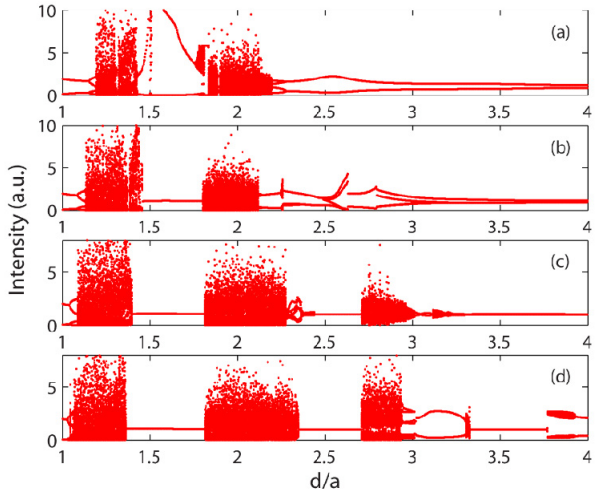

Fig. 4. One-parameter BDs as a function of laser separation d/a, calculated from laser A for different frequency offsets in the structure in the last line of Table 1. (a) $\Delta\Omega/2\pi = -5$ GHz, (b) $\Delta\Omega/2\pi = -3$ GHz, (c) $\Delta\Omega/2\pi = -1$ GHz, and (d) $\Delta\Omega/2\pi = 0$ GHz. Those for laser B are similar. Other parameters are $P = 1.1P_{th}$ and $\alpha_H = 2$.

Optics EXPRESS

We have shown that the laser separation and waveguiding structures have significant effects on the system dynamics. Next we consider the impact of a static offset in frequency between laser A and B. As an example, we show in Fig. 4 several BDs as a function of d/a in the case of real index antiguide with $\Delta n = -0.0005$ and gain-guiding for different values of frequency offset. For comparison purposes, the result in Fig. 3(d1) for the case of zero offset is repeated in Fig. 4(d). As shown in Fig. 4, the windows of phase-locked solutions and chaotic regions become fewer when the frequency difference between the two lasers becomes larger. For sufficiently large offset, phase-locked solutions no longer exist for the considered interval of d/a since no supercritical saddle-node bifurcation can be encountered; see Fig. 4(a). These results indicate that, given a waveguiding structure, the frequency offset also has a significant influence on the dynamics of the two-laser array in the absence of injection.

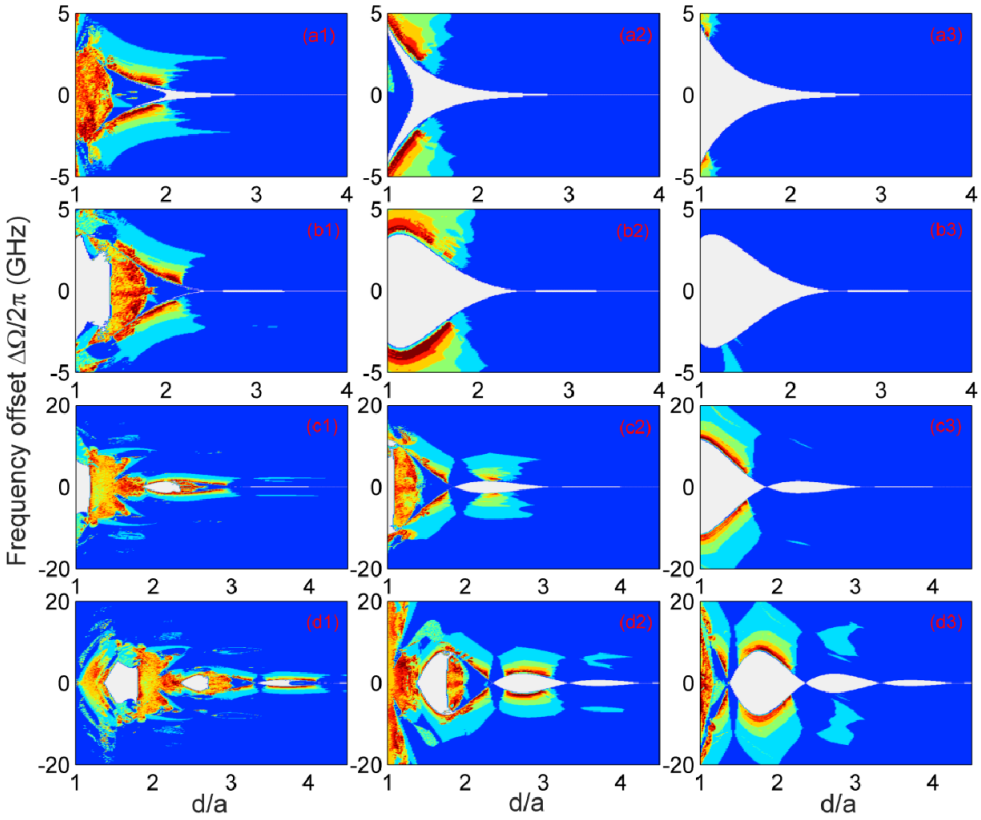

Fig. 5. Two-parameter BDs in the $(d/a, \Delta\Omega/2\pi)$ plane in the solitary two-element laser array, where $\alpha_H = 2$. From top to bottom: cases described in sequence of lines from top to bottom of Table 1. From left to right: $P = 1.1P_{th}$, $2P_{th}$ and $5P_{th}$. The color code marks the number of extremal values (maxima and minima) of the intensity time series in laser A. The white indicates phase-locked solutions, dark blue shows period-one oscillation, light blue marks period-two oscillation, and other colors represent complex dynamics.

3.2 Two-parameter bifurcation diagrams

To provide a more complete picture of the parameter dependence of the laser dynamics, two-parameter BDs as a function of the laser separation ratio d/a and laser frequency offset $\Delta\Omega/2\pi$ are calculated in this section. The BDs obtained by direct integration are summarized in Fig. 5, for the four waveguiding structures and with constant $\alpha_H = 2$. To visualize the

Optics EXPRESS

impact of the pump level on the resulting BDs, three values of normalized pump levels are considered; $1.1P_{th}$ (left column), $2P_{th}$ (middle column) and $5P_{th}$ (right column). In these maps, the different dynamical regimes are identified from the extrema of the intensity time series, in which steady-state (white), period-one (dark blue), period-two (light blue), and complex dynamics (other colors) are identified as a constant intensity, two intensity extrema, four intensity extrema, and even more extrema, respectively [30]. Since the results for laser A and B are quite similar, only those for laser A are shown in the maps. However, it is worth noting that two-parameter BDs obtained from laser A show certain asymmetry about the frequency offset $\Delta\Omega/2\pi$ = 0 GHz, whilst those for laser B should exhibit mirror/opposite asymmetry about this offset, which can be expected from the rate equations.

The BDs reveal importance of the waveguide structures in determining the overall behavior, and several interesting features can be deduced in the (d/a, $\Delta\Omega/2\pi$) plane. First, there is a single uninterrupted locking region in the cases of real index guide with $\Delta n = 0.000971$ and real index guide with $\Delta n = 0.0005$ and gain-guiding, while two uninterrupted locking regions are seen in the case of pure gain-guiding ($\Delta n = 0.0$) and three uninterrupted locking regions are visible in the case of real index antiguide with $\Delta n = -0.0005$ and gain-guiding. These regions are bounded by the saddle-node or Hopf bifurcations predicted in [38], which agree well with the boundaries of steady-state operation shown in these two-parameter BDs. Second, such visualization uncovers regions of complex dynamics which are important for modern applications of lasers that may require chaos rather than steady-state emission. Several distinct regions of these dynamics are found for the cases of pure gain-guiding ($\Delta n = 0.0$) and real index antiguide with $\Delta n = -0.0005$ and gain-guiding. Third, both locking and complex dynamics regions are concentrated around small frequency offsets and are almost symmetric with respect to frequency offset $\Delta\Omega/2\pi$ = 0 GHz. Note here that one may observe a certain degree of asymmetry in these BDs. This can be explained by the multistability in our laser system as well as the imperfection of our automated computational protocol for distinguishing different dynamical regions (for example, in the case of extremely small but non-negligible amplitude oscillations). However, this has no significant influence on the conclusion we can draw from the two-parameter BDs. Finally, as the pump is increased, the locking region expands, while the regions of complex dynamics shrink in size and even disappear.

It should be pointed out that the fact that the regions of complex dynamics are suppressed as the pump rate increases is opposite to the evolution of the laser dynamics observed in semiconductor lasers subjected to conventional optical feedback, where instabilities of the laser persist and never disappear for the increase of the pump rate [44]. However, one can also find features similar to our case in other laser systems [44], such as a polarization-rotated feedback configuration and an optical injection system, despite originating from different mechanisms. In the two-laser array studied, with increasing the pump rate, the basic bifurcations, i.e., saddle-node and Hopf, expand, resulting in larger regions allowing the existence of phase-locked solutions, and beyond that, the web of further bifurcations (such as Torus, period-doubling, and saddle-node of limit cycle) becomes simpler. All these boundaries of various dynamics can be exactly matched with those bifurcations obtained from the continuation technique (not shown here; however, some examples of the basic bifurcations are discussed in [38]). Thus, one can expect more limited complex dynamics in the laser array for the considered coupling parameters and larger values of the pump rate.

Optical chaos from a laser has many potential applications, for example, it can be used as the broadband carrier in secure communication [32]. Therefore, it is of vital importance to identify the regions with chaotic dynamics in the maps. In Fig. 5, the number of intensity extrema was used to distinguish different dynamic regions; however, a large value of this measure does not necessarily indicate chaotic emission. For this reason, we employ the 0-1 test for chaos to separate chaotic emission from nonchaotic emission [45]. This calculation is

Optics EXPRESS

fast and easy to implement and interpret, giving a result of 1 for chaos and 0 for other dynamics. For illustrative purpose, we present the two-parameter BDs for $P = 1.1P_{th}$ and a large linewidth enhancement parameter, α_H = 6, in the cases of real index guide with $\Delta n = 0.0005$ and gain-guiding and real index antiguide with $\Delta n = -0.0005$ and gain-guiding, as shown in Figs. 6(a) and 6(b), respectively. The corresponding results for the 0-1 test for chaos are displayed side by side, as shown in Figs. 6(c) and 6(d). A comparison between these two types of maps shows that our BDs provide a surprisingly accurate prediction of chaos and the two-laser array allows for chaos generation in wide regions of the parameter space. In addition, as compared to Figs. 5(b1) and 5(d1) for α_H = 2, there is no noticeable difference in the appearance of the overall structure of all the dynamical regions. However, a large value of α_H enlarges the proportion of complex dynamics in the parameter space, which is a common feature observed in all semiconductor laser systems.

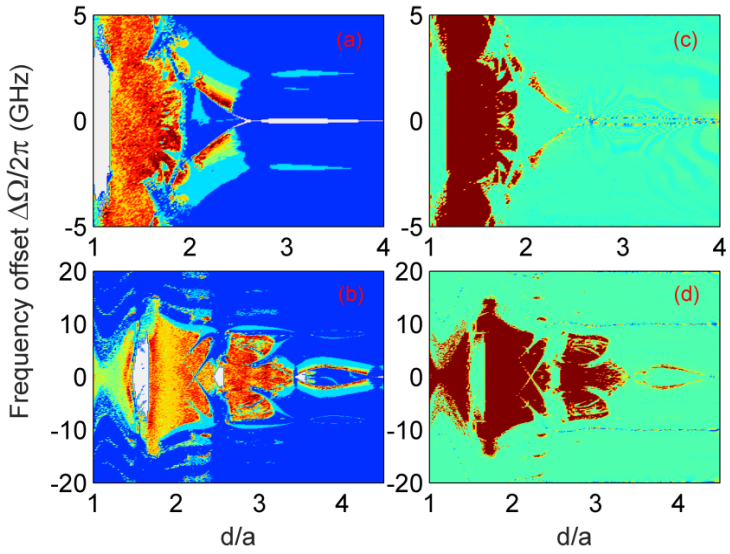

Fig. 6. Comparison between the (a, b) bifurcation diagrams and (c, d) maps obtained by 0-1 test for chaos in the $(d/a, \Delta\Omega/2\pi)$ plane. (a,c) case of second line in Table 1; (b,d) case of last line in Table 1. Other parameters are α_H = 6, $P = 1.1P_{th}$. On the left panel: the white indicates phase-locked solutions, dark blue shows period-one oscillation, light blue marks period-two oscillation, and other colors represent complex dynamics; on the right panel: red stands for chaos and others nonchaotic.

Sustained periodic oscillation is another interesting feature observed in laser arrays, and some examples are shown in Fig. 1(c) and Fig. 2. In the two-parameter BDs, such period-one oscillation, marked with darker blue color, occupies a large proportion in the parameter space, as shown in Figs. 5 and 6. The oscillation frequency in this area is of interest and discussed in [12,15], where it is associated with the relaxation oscillation resonance for weak coupling (large laser separation) in the case of zero laser frequency offset. In contrast for the non-zero case, we have found that the oscillation frequency is dominated by frequency offset between laser A and B, particularly if the separation between the two lasers is sufficiently large. For smaller separation the oscillation frequency is increasingly influenced by the complex coupling coefficient shown in Fig. 2 of [38]. Two examples of the frequency variation versus d/a are shown in Figs. 7(a) and 7(b), which correspond to the cases of real index guide with $\Delta n = 0.0005$ and gain-guiding and real index antiguide with $\Delta n = -0.0005$ and gain-guiding, respectively. It is clear that the results in Fig. 7 just confirm that the oscillation frequency

Optics EXPRESS

tends towards the offset frequency($f_{ROF} = 4.5$ GHz and $f_{ROF} = 4.1$ GHz at $P = 1.1P_{th}$ for these two waveguides, respectively), in contrast to the case considered in [12,15] for zero offset.

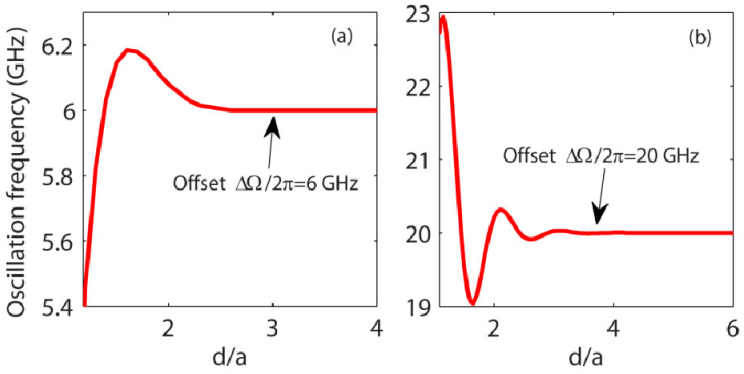

Fig. 7. Oscillation frequency as a function of *d/a*; (a) case described in the second line of Table 1, $\Delta\Omega/2\pi = 6$ GHz ; (b) case described in the last line of Table 1: $\Delta\Omega/2\pi = 20$ GHz . Other parameters are $P = 1.1P_{th}$ $\alpha_H = 2$.

Figure 8 shows the oscillation frequency and peak-to-peak amplitude in the (d/a , $\Delta\Omega/2\pi$) plane, where the results for the case of gain-guiding and real index antiguide with $\Delta n = -0.0005$ are taken as an example. In Fig. 8(a), only the frequency of period-one oscillation is displayed, and interestingly, in almost all cases with finite offsets (with a slight exception for those close to zero offset), the calculated frequency is close to that of the offset. Nevertheless, one can see some variation of the frequency for relatively closer laser separation (see the range for $d/a < 2$). In addition, we show the peak-to-peak normalized amplitude calculated for all the dynamical regimes in Fig. 8(b). As expected, regions with complex dynamics exhibit large-amplitude oscillations, and the amplitude of the period-one oscillation of interest here decreases as the laser separation increases.

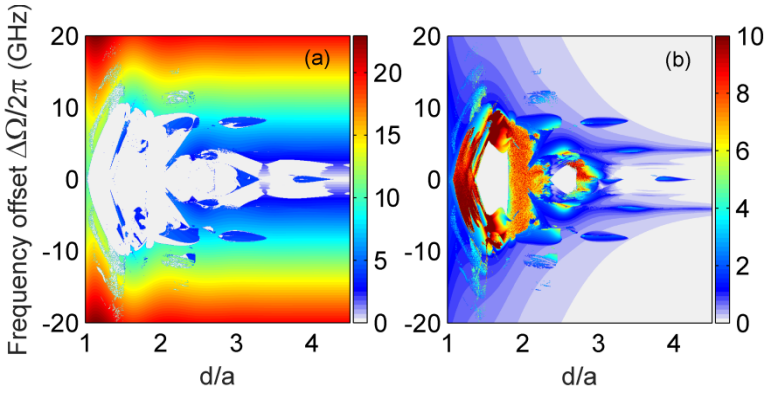

Fig. 8. (a) Oscillation frequency (GHz) and (b) normalized amplitude in the $(d/a, \Delta\Omega/2\pi)$ plane for the case described in the last line of Table 1. Parameters are $P = 1.1P_{th}$, $\alpha_H = 2$. On the left panel: white color means the non-period one region.

Optics EXPRESS

4. The influence of optical injection

The studies so far have been focused on a solitary pair of laterally-coupled semiconductor lasers. The two lasers show similar behaviors due to the symmetrical properties of the whole system. In this section, we investigate the two elements of the laser array under asymmetrical operation conditions, that is, one of the two lasers (laser A) is subjected to an additional optical injection from a third laser. As discussed in [16], external optical injection has been employed to stabilize the phase-locking in two-laser arrays, and in [39] we have carried out a comprehensive analytical and numerical study on the injection locking conditions and bandwidth. Here the rich dynamical regions outside the locking region in two laterally-coupled semiconductor lasers in the presence of optical injection are investigated.

In common with other optically injected systems [24,26–28,46], two important controllable parameters are; the injection strength K defined as K_{inj}/Y_{AS}, where K_{inj} is defined in Eq. (8) and Y_{AS} is the mean steady-state value of Y_A, and the frequency detuning $\Delta\omega_{inj} = \omega_{inj} - \Omega_A$ between the injected light and that of laser A in the absence of injection. We are interested in dynamics of both laser A and laser B in the parameter plane spanned by the injection parameters K and $\Delta\omega_{inj}$, so that two-parameter BDs in the (K, $\Delta\omega_{inj}/2\pi$) plane are calculated by directly integrating the rate equations.

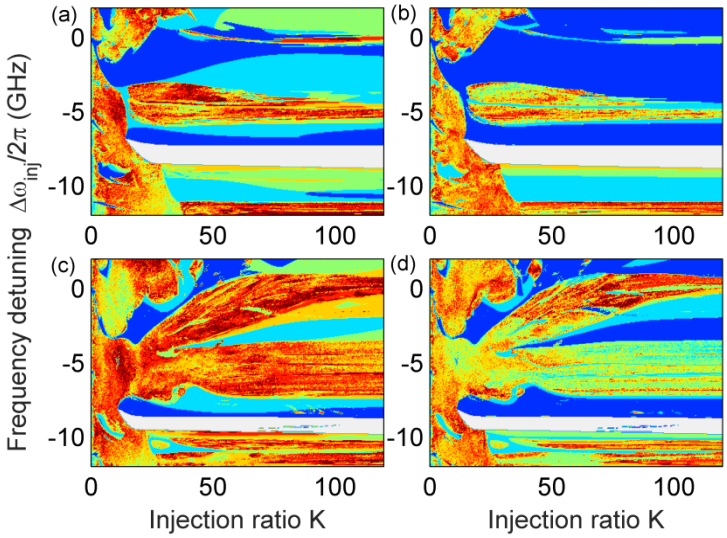

Fig. 9. Two-parameter BDs in the $(K, \Delta\omega_{inj}/2\pi)$ plane, with case described in the second row of Table 2. (a) α_H = 2; (b) α_H = 3. Other parameters are $P = 1.1P_{th}$, $\Delta\Omega/2\pi = -6$ GHz, $d/a = 1.2$. (a,c) results for laser A and (b,d) laser B.

Figures 9(a) and 9(b) display typical examples of BDs in the (K, $\Delta\omega_{inj}/2\pi$) plane for laser A (left) and laser B (right) in the optically injected two-element laser array, where $P = 1.1P_{th}$, α_H = 2, and d/a = 1.2. For this case we select the waveguide with real index guide with $\Delta n = 0.0005$ and gain-guiding and an offset of $\Delta\Omega/2\pi = -6$ GHz between laser A and laser B. Outside the locking region, optical injection destabilizes the phase-locked solutions and the system undergoes various bifurcation scenarios, giving rise to more complex dynamics, such as multiperiodic, quasiperiodic and chaotic oscillations. Moreover, the two lasers may yield different dynamics for the same set of parameters; for example, laser A operates in period-two oscillation while laser B is in period-one oscillation and vice versa.

Optics EXPRESS

We attribute this to the combined effect of weak coupling between the two lasers and the asymmetric operation condition, where only laser A is subject to external optical injection. Behavior of this type is never found in the solitary laser array.

In the case of a solitary two-element laser array, large values of linewidth-enhancement factor have been found to enlarge the regions of complicated dynamics. Here, in the presence of injection, we show the effect of an increase in α_H to 3, as shown in Figs. 9(c) and 9(d). It is clearly seen that both lasers can still be injection-locked in a well-defined region, but the extent of complex dynamics is greatly increased compared to the former case of $\alpha_H = 2$. In the maps shown in Fig. 9, we have presented results for a frequency offset between the two lasers of −6 GHz. This is tunable, and, as indicated in our previous work [39], one can always observe an injection-locking region close to the chosen offset. However, in Fig. 9 we see that outside the locking region are extensive regions of complex dynamics, and we observe this general behaviour for all values of offset and with all of the waveguiding structures listed in Table 1. Such regions are comparatively insensitive to injection strength and frequency detuning, thus making them relatively easy to excite.

Lastly, we emphasize that the existence of asymmetry in the oscillation amplitude of the laser array where only one element is subjected to optical injection can be observed in all the waveguiding structures. Controllable asymmetric phase-locked states of the fundamental active photonic dimer consisting of two mutually-coupled semiconductor lasers have been reported [22]. However, in that paper, the studies were focused on the steady-state solutions and the use of inhomogeneous pumping. In contrast, we concentrate on the dynamic regimes in two laterally-coupled semiconductor lasers homogeneously pumped and in the presence of optical injection (another kind of asymmetric condition). To quantify the similarity and difference between the oscillation amplitudes of the two lasers, we introduce the contrast ratio as $C = (\Pi_A - \Pi_B)/(\Pi_A + \Pi_B)$, where $\Pi_{A,B}$ are peak-to-peak amplitudes of laser A and laser B, positive values of C mean that laser A oscillates with a larger amplitude than laser B, while negative values represent the opposite. For perfectly equal amplitudes, the contrast ratio becomes $C = 0$, while the larger the value of $|C|$ the bigger the difference in amplitudes.

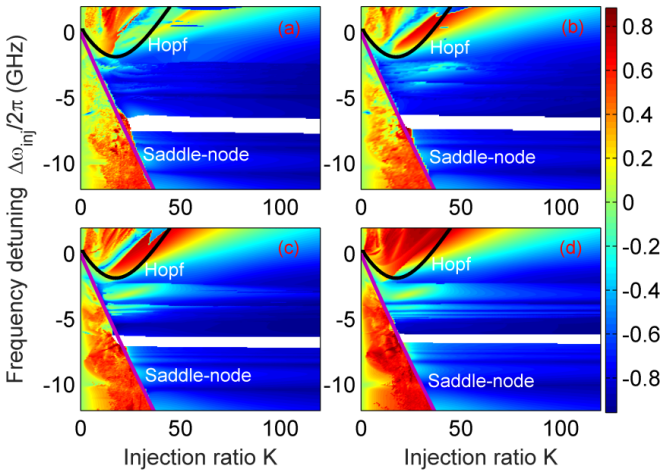

Fig. 10. Amplitude comparison in terms of the contrast ratio C between the two lasers in the $(K, \Delta\omega_{inj}/2\pi)$ plane; (a) Case of line 1 of Table 1, d/a = 1.2; (b) Case of line 2 of Table 1, d/a = 1.5; (c) Case of line 3 of Table 1, d/a = 2.2; (d) Case of line 4 of Table 1, d/a = 3.2. Other parameters are $P = 1.1P_{th}$ and $\alpha_H = 2$. Hopf and saddle-node bifurcation curves for a single laser subjected to injection are shown.

Optics EXPRESS

Figure 10 is computed for the four cases of waveguiding structures listed in Table 1, and displays a representative example of the calculated contrast ratio C in the (K, $\Delta\omega_{inj}/2\pi$) plane, where d/a is chosen to ensure weak coupling in each case. In these maps, the steady-state injection locked region is depicted in white, where C is not calculated. As seen in this figure, there is an interesting phenomenon: in a well-defined region ($C < 0$), laser B oscillates with a much stronger amplitude than laser A, while in the remaining regions, the oscillation amplitude of laser A can be larger than or comparable with that of laser B. It is worth noting that the former (blue color) region almost coincides with the injection-locking region in the case of a single slave laser subjected to optical injection; see the region confined by the saddle-node and Hopf bifurcation curves indicated in the figure. In this region laser A is injection-locked by the external light (continuous wave) in the absence of laser B. This means that laser A tends to yield continuous wave because of injection locking from external light. Even though laser B starts to interact with laser A, weak coupling between them is not enough to compensate for the locking effect and a weaker amplitude is thus expected for laser A. The above results show interesting similarities and differences (asymmetry) between the oscillation amplitude of the laser array in the presence of optical injection.

5. Conclusion

In summary, we have numerically investigated the nonlinear dynamics in two laterally-coupled semiconductor lasers in the absence and presence of external injection. We focus on the case weak coupling where coupled-mode theory is sufficiently accurate, and utilize direct integration of rate equations to model the system. For the solitary pair of coupled lasers both one-parameter and two-parameter BDs have been used to visualize the dynamic variation in the parameter space, where phase-locked, periodic, and chaotic regions are of interest and revealed in some detail. Our results highlight the importance of static waveguide design on these dynamic states, and the engineering possibilities for such a coupled system. Parameters such as the laser spacing, frequency offset and linewidth enhancement factor are shown to have strong effects. Our analysis has been restricted to the case of equal pumping of each laser; the effects of asymmetric pumping have yet to be explored.

In addition we examined the effect on the dynamic behavior of introducing optical injection into one of the lasers. Two-parameter BDs were employed to map out the dynamic regimes outside the injection-locked region. The external injection is seen to have a major impact on the system, significantly altering the nature and regions of dynamics. In conjunction with static waveguide design, controlling both the injected power and frequency detuning could be used to either make or break the symmetry between the coupled lasers and alter their outputs. Chaotic regions in particular could be significantly enlarged, thus offering a large operational parameter space, attractive for practical use. Moreover the output of the two lasers could be varied both in terms of their relative intensity and their dynamics, offering switching behavior via the external input. If these results could be extended to larger arrays then this would open up the possibility of using such a system for spatial signal distribution or processing. Moreover the ability to control the nature of the dynamics could find applications in random number generation, chaotic communication or spatial pattern generation.

Funding

Engineering and Physical Sciences Research Council (Grant No. EP/M024237/1).